

Hot Pixels as a Probe of WFPC2 CTE Effects

J. Biretta and V. Kozhurina-Platais
July 15, 2005

ABSTRACT

Hot pixels provide a potentially useful probe of CTE effects, as they can be used to measure effects at the smallest scales -- at single pixel level. Herein we outline a method of using the tails on hot pixels to quantify CTE effects, and apply it to CTE tails in WFPC2 dark frames. As we show, many of the behaviors associated with photometric CTE are also found for hot pixel tails including the dependences on CCD row, epoch, and target brightness. The brightness distribution of the tails are well fit by a sum of exponential decays with scale-lengths of 0.6, 6, and 96 pixels, with the vast majority of the counts being in the longest decay component. The integrated counts in the tail are nearly equal to the expected photometric CTE, suggesting these tails are in fact the photometric deficit. We also find significant tails near row zero ($y=0$), and show these tails would cause effects quantitatively similar to the "long vs. short" effect. Finally we show evidence for chip-to-chip differences in CTE with WF4 having the least CTE.

Introduction

Charge Transfer Efficiency (CTE) problems are perhaps the most important single issue for CCD detectors on-board HST. While CCDs have high quantum efficiency, any errors or inefficiencies during charge transfer and readout will reduce the detected counts, and hence adversely affect photometric accuracy and detection of faint targets. As CTE errors increase with time on-orbit, it may ultimately limit the scientifically useful lifetime of instruments. Considerable effort has already gone into the study of CTE. Its impact on both stellar photometry (Whitmore, Heyer, Casertano 1999; Heyer 2002; Dolphin 2002;

Whitmore & Heyer 2003) and extended targets (Riess 2000) has been studied. Previously cosmic rays have been used a diagnostic of their growth rate (Riess, Biretta, Casertano 1999, hereinafter RBC99). Herein we investigate hot pixels as a useful probe of CTE effects.

Hot pixels have the potential to provide unique insights to CTE, since they represent isolated bright pixels, and hence allow study of CTE at the single-pixel level. This type of information might be useful in studying the detailed physics of CTE as well as efforts to correct CTE effects at the pixel level (e.g. Bristow, et al. 2002). Both stellar photometry and studies of cosmic rays, while extremely useful, deal with clusters of bright pixels, and hence possibly obscure details such as the shape of the tail, and its detailed dependence on pixel brightness. Furthermore, some issues such as absolute CTE losses and detector-to-detector variations might be obscured by the measurement technique. For example, photometric CTE is typically measured by differencing results for a target as it is moved around the CCD, or by differencing results for different detectors, thus potentially obscuring important information about *absolute* losses or detector dependences.

Imperfect CTE is thought to be caused by a charge-trapping effect in the CCDs. This model is suggested by the residual images sometimes seen subsequent to bright exposures (Biretta, Ritchie, Rudloff 1995; Biretta and Mutchler 1997; Baggett, Biretta, Hsu 2000), and by tails sometimes seen on bright, isolated targets images. In this model, some small amount of charge is left behind or “trapped” as the image is moved across the CCD to the readout amplifier. At some later time the charge is released, hence producing the various artifacts mentioned. In the case of tails on images, the release timescale is short (i.e. few to many CCD vertical clockings, or 10s of milliseconds), whereas the residual images represent charge which is released in longer timescales (i.e. long compared to the CCD readout time of one minute).

Important aspects of the photometric effects are also readily explained in such a picture. CTE reduces the photometric counts in images, since charge is robbed from the relatively small apertures used for photometry. Trapping also explains the increased charge deficits for targets farther from the readout amplifier, as more traps are encountered during the larger traverse across the CCD during readout.

Herein we study hot pixel tails as a potential metric of CTE effects. We examine the general properties of the hot pixel tails, compare these against the properties already established for photometric CTE, and finally illustrate several new properties of CTE revealed by analysis of hot pixels.

Method

The process is relatively simple. First a “monthly dark” is computed for a given epoch. Typically 20 to 30 routine 1800 second WFPC2 darks are combined to remove cosmic rays in the standard way using MKDARK. In an effort to minimize changes occurring across the 20 images, they are selected to be bounded by a pair of WFPC2 monthly decontaminations. Hence each “monthly dark” will typically span 30 contiguous days.

Next this monthly dark is processed through specialized software which identifies hot pixels, extracts the tail on each one, and finally averages and sums the tails. In practice we identify any pixel whose value exceeds 100 DN^1 in the monthly dark as a hot pixel (this value is merely used for convenience; any other value or range in values could have been used). For each hot pixel at say (x, y) the brightness profile in pixels (x, y) through $(x, y+40)$ is extracted from the image. Since we were concerned that the derived profile might be corrupted if other hot pixels were present in the tail, we rejected any hot pixels where a pixel in the tail exceeded some threshold.² We also compute and subtract a local background from each hot pixel tail; we use columns $x-4$, $x-3$, $x+3$, and $x+4$ adjacent to the tail as background regions, computed the median background brightness³, and then subtract this from the tail for the hot pixel at (x, y) . In this same way, the profile of each hot pixel in the image is extracted and background subtracted, and finally all the extracted hot pixel tails are averaged to produce an effective brightness profile of the hot pixel tail.⁴

While we will often use all the hot pixels in an image, it is also possible to select only those on a given CCD, those within some area of the CCD, or those where the hot pixels lie in some brightness range. In this way, it is possible to examine various dependencies of the CTE such as CCD, y -position on the CCD, or pixel brightness. In all cases we will avoid using pixels near the CCD edges ($20 > x > 780$ and $50 > y > 750$) since artifacts are more prevalent there.

-
1. “DN” used herein indicates the number of detected counts at gain of 7 electrons per DN.
 2. In practice we used a position-variable threshold. The hot pixel was rejected if the pixel immediately above it exceeded 10DN , or if the pixel 2 pixels above it exceeded 5 DN , or if any of the other pixels in the tail exceeded 2.5DN . At late epochs where CTE is large, this threshold may need to be adjusted to higher levels to avoid excluding hot pixels with strong tails.
 3. The background level was determined in an iterative fashion by rejecting pixels greater than 2.5 sigma from the median, and then repeating the process.
 4. Hot pixels will have weak tails even in the absence of CTE due to readout effects, but the intensity is negligible and we have not made any corrections for it. During the readout process the image is “clocked” down the CCD, and hence all pixels above the hot pixel will receive a small contribution from it. The effective exposure time for this readout effect is approximately the chip readout time of 13.6 sec divided by 800 rows, or 0.017 seconds; this is only 10^{-5} of the 1800 sec exposure time for these dark frames. Hence the tail contributed by this effect for the average 310 DN hot pixel is only 0.003 DN per pixel. As we will see, this intensity is completely negligible compared to CTE.

In most cases we will examine only the first 40 pixels of the tail (i.e. pixels (x, y) through $(x, y+40)$ or expressed another way, $\Delta y=1$ to $\Delta y=40$), though we will sometimes also examine the more extended tail covering $\Delta y=1$ to $\Delta y=200$. In either case, the analysis methods are essentially identical.

Since we will use hot pixels to study CTE growth, an immediate question is how the hot pixels themselves vary over time. Figure 1 and Figure 2 show the number of hot pixels ($>100\text{DN}$) and their average strength as functions of time for all four CCDs. While the number of hot pixels increases with time, presumably due to radiation damage in the CCDs, the average strength remains relatively constant. Hence we ignore the brightness change of the hot pixels themselves, when using them to study the evolution of CTE effects.

Figure 1: Number of hot pixels vs. epoch.

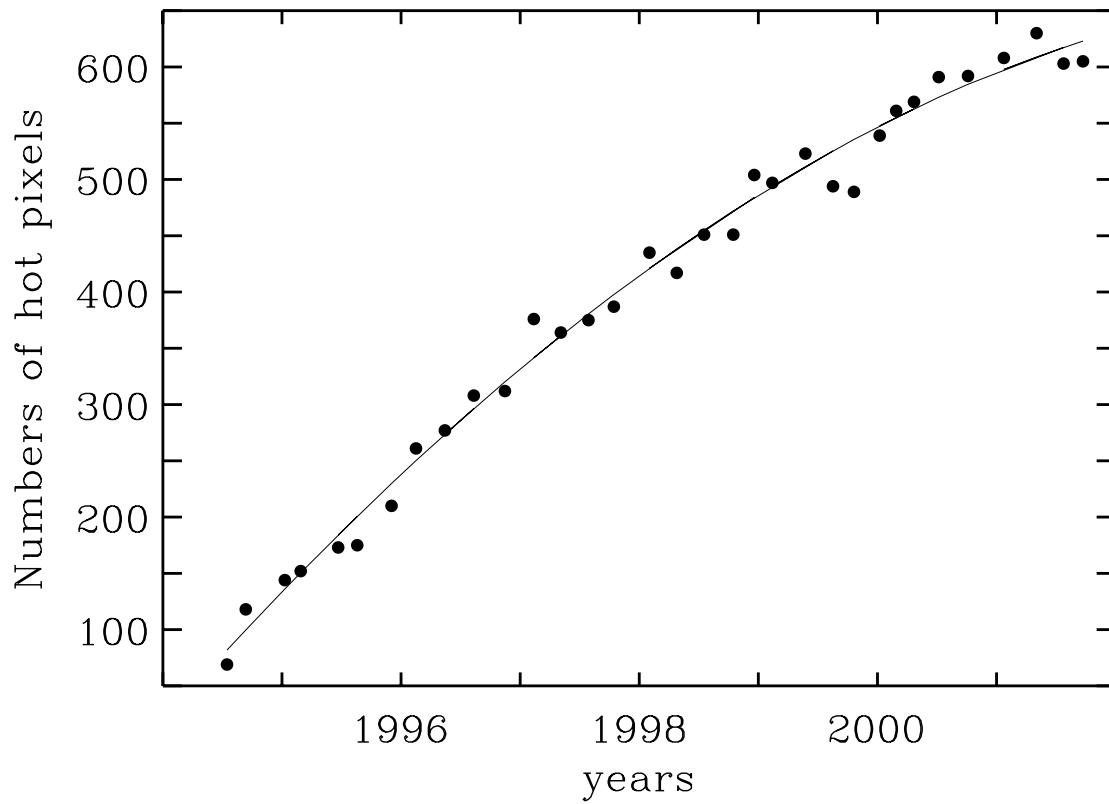
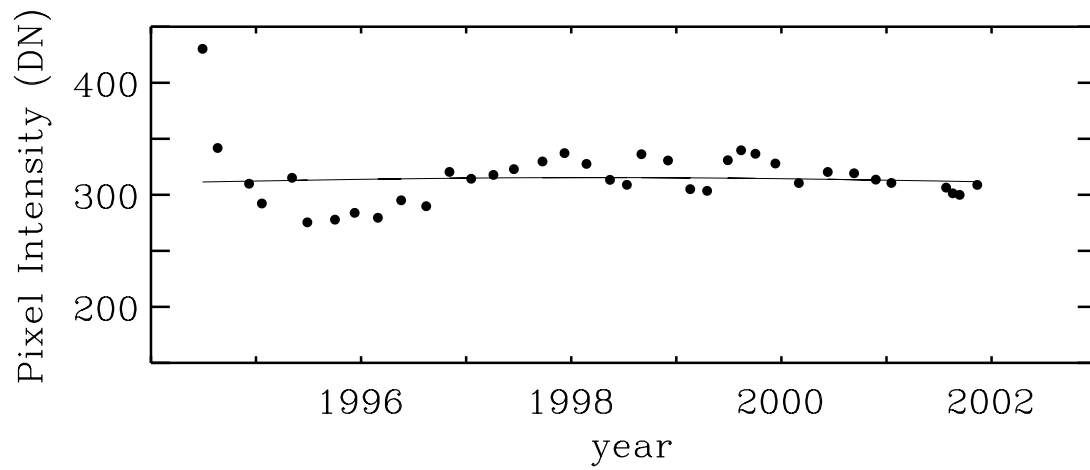


Figure 2: Average brightness of hot pixels vs. epoch.



Results

Shape and extent of CTE tail

It is interesting to know the shape and length of the CTE tail. This, for example, might impact one's choice of aperture when performing photometry, or might lead one to use a model PSF which includes an appropriate tail. Figure 3 illustrates the impact of CTE on a single bright pixel -- counts are displaced from the correct image location into a pair of tails extending into the +x and +y directions. This image was made by stacking ~700 hot pixels extracted from WFPC2 dark frames.¹ Rapidly decaying tails are seen in both the +x and +y directions. However, the +y tail has an additional faint component with a very slow decay (lower panel in Figure 3), and in fact this slowly decaying +y tail contains the majority of the displaced counts, and will be the focus of our discussion.²

Figure 4 illustrates the average hot pixel tail in the +y direction for years 1994, 1997, and 2001. Each profile is the average hot pixel tail drawn from four³ monthly darks spread uniformly through the respective year. Data are taken from all four CCDs, and hot pixels in the range 100 to 4000 DN are used. For 1994 about 200 hot pixels are represented in the profile, while for 2001 about 2400 hot pixels are represented. Since we have used nearly the entire area of each CCD, the profiles effectively represent the hot pixel tail near the center of the CCD (i.e. row $y=400$).

For example, the 1994 data show that the first pixel above the hot pixel (i.e. at $y+1$) averages 0.7 DN above the background; the second pixel above the hot pixel ($y+2$) averages 0.14 DN above the background, and so forth. As one might expect, the strength of the CTE tail increases with time. While the tail is very weak in 1994, it is quite significant by 1997; and by 2001 it is roughly twice the 1997 strength. It is also apparent that by 2001 the tail extends past the 40 pixel window we have plotted (i.e. past $\Delta y=40$).

The "half-life" of the decay with y distance appears roughly constant. For example, the 1997 curve decays by a factor of two between $\Delta y=5$ and $\Delta y \sim 22$ (Figure 4), and the 2001 curve decays by a factor two between $\Delta y=5$ and $\Delta y \sim 18$. Hence the longer apparent tail in 2001 is primarily attributable to increasing strength, rather than increasing decay length.

-
1. Hot pixels in the brightness range $100 < \text{DN} < 4000$ were taken from all four CCDs.
 2. Detailed study of the X-CTE or serial tail is left for future reports.
 3. Only three superdarks are averaged for 1994.

Figure 3: Stacked image of ~700 hot pixels extracted from WFPC2 dark frames taken in late 1999; bottom panel is same image enhanced to show faint pixels.

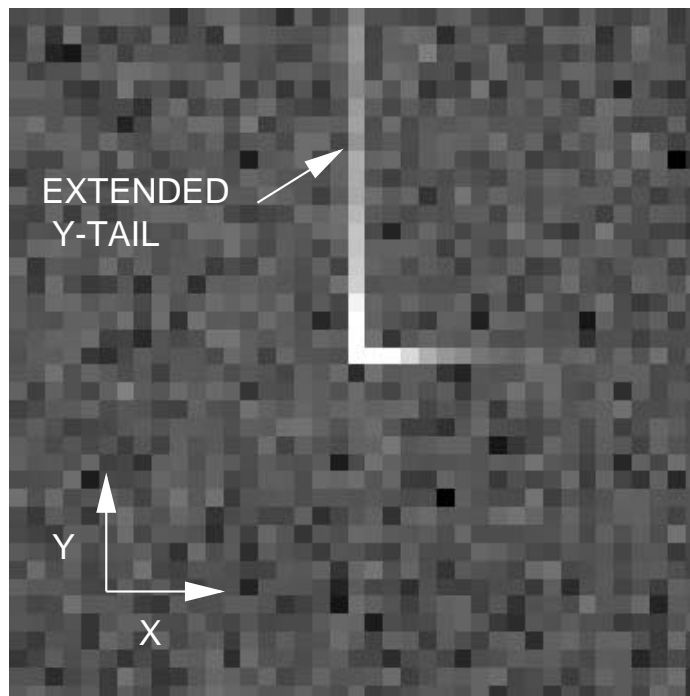
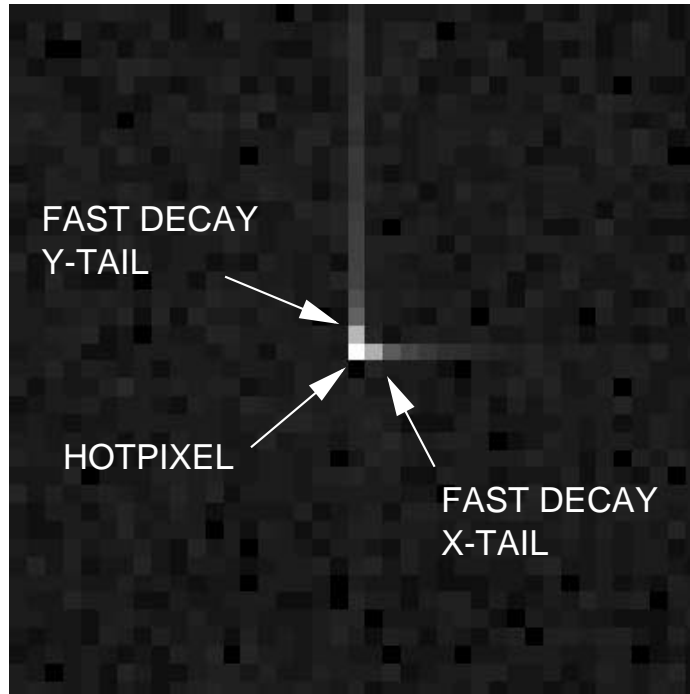
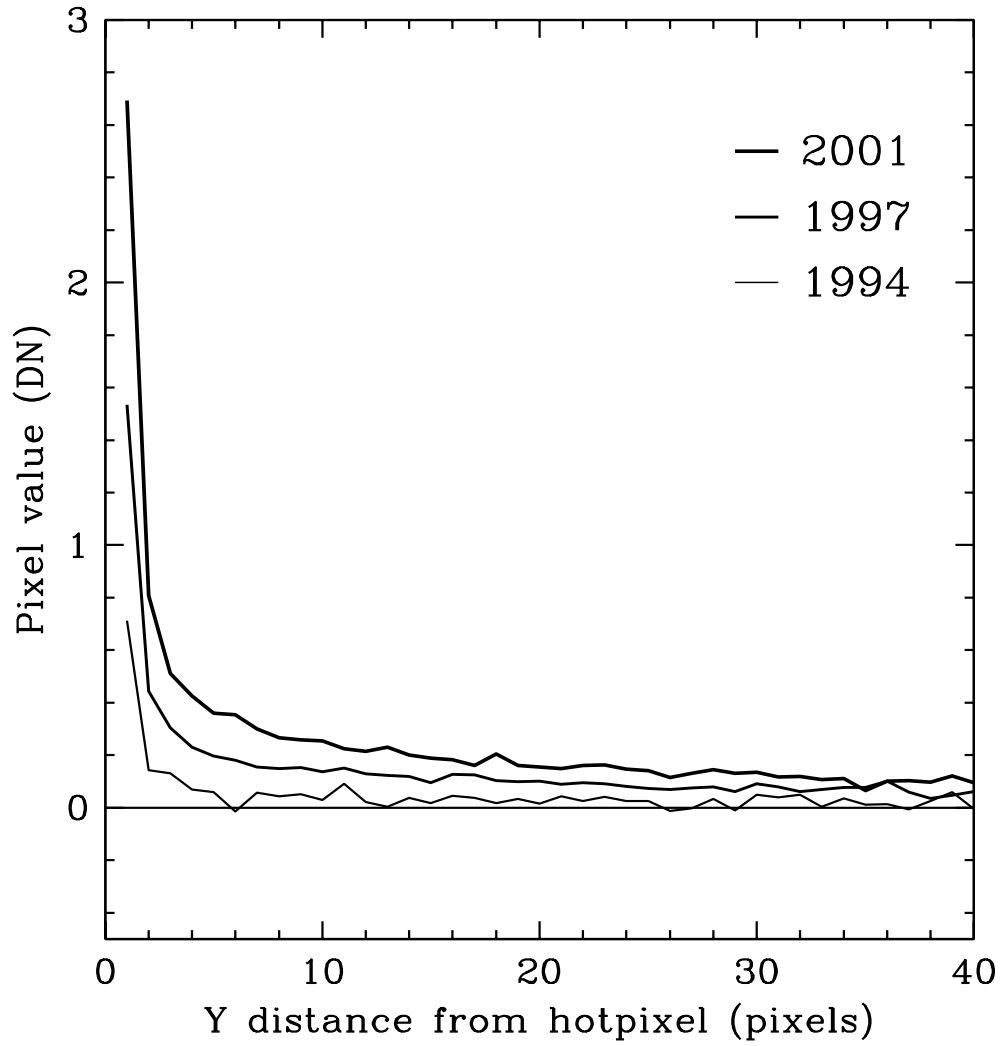


Figure 4: Average WFPC2 hot pixel tails for years 1994 (lower line), 1997 (middle line), and 2001 (upper line).



In an effort to more precisely describe the profile, we have fit functions to it consisting of a double exponential plus constant:

$$I(\Delta y) = a_1 e^{-\frac{\Delta y}{a_2}} + a_3 e^{-\frac{\Delta y}{a_4}} + a_5$$

where Δy is the distance along the tail from the hot pixel. A single exponential decay term did not give a good fit. Multiple exponentials seem plausible if there are multiple decay processes at work, each having its own decay length-scale. Obviously the constant term is unphysical, but it likely implies a third decay term with a very long decay length compared to our 40 pixel region we are fitting. The fits for 1997 and 2001 are shown in Figure 5 and Figure 6, respectively, and the fit parameters are given in Table 1. Appar-

Table 1. Fits to averaged hot pixel tails for 1997 and 2001 (gain 7).

Epoch	a_1 (1st coeff, DN)	a_2 (1st decay scale, pixels)	a_3 (2nd coeff, DN)	a_4 (2nd decay scale, pixels)	a_5 (constant term, DN)
1997	7.9 ± 1.0	0.55 ± 0.04	0.24 ± 0.03	9.7 ± 2.0	0.06 ± 0.008
2001	13.8 ± 1.0	0.54 ± 0.02	0.46 ± 0.03	9.1 ± 0.9	0.102 ± 0.008

ently the shape of the tail is remarkably constant with time. For both epochs the first exponential has a decay scale of about 0.55 pixel, while the second has a scale of about 9 pixels. The two coefficients and constant term all increase by similar factors between 1997 and 2001; the increases are 1.75 ± 0.24 , and 1.91 ± 0.26 , and 1.70 ± 0.26 , respectively for a_1 , a_3 , and a_5 . Again, this indicates the overall shape of the tail appears to be preserved as CTE increases. We note this behavior is similar to that for nuclear decay, where the half-life is invariant and independent of the count rate.

In an effort to better quantify the behavior at large Δy , we processed four 2002 monthly darks with a limit of $\Delta y=200$ pixels, instead of $\Delta y=40$ pixels. The averaged profile is shown in Figure 7. The profile is noisier than the previous profiles, since only the center 400 rows of the CCD can be used¹ (i.e. $y=200$ to 600), and hence fewer hot pixels are averaged. We have fit a triple exponential decay to this profile of the form:

$$I(\Delta y) = a_1 e^{-\frac{\Delta y}{a_2}} + a_3 e^{-\frac{\Delta y}{a_4}} + a_5 e^{-\frac{\Delta y}{a_6}}$$

1. For pixels $Y>600$ the tail would be truncated by the CCD edge at $Y=800$. We also discard hot pixels at $Y<200$, so as to maintain the effective average location of $Y=400$ for the hot pixels.

and the results are given in Table 2. The first decay length is similar to that found previ-

Table 2. Fit to averaged hot pixel tail for epoch 2002 (gain 7) with $\Delta y=1$ to 200.

Epoch	a_1 (1st coeff, DN)	a_2 (1st decay scale, pixels)	a_3 (2nd coeff, DN)	a_4 (2nd decay scale, pixels)	a_5 (3rd coeff, DN)	a_6 (3rd decay scale, pixels)
2002	12.5 ± 0.8	0.59 ± 0.02	0.55 ± 0.05	5.9 ± 0.6	0.246 ± 0.008	96 ± 4

ously, but the second decay length is shorter, ~ 6 pixels instead of ~ 9 pixels. The third decay scale is 96 pixels.¹

It is interesting to examine the fraction of the total CTE in each of these exponential components. Simply integrating the three exponential functions from $\Delta y=1$ to infinity for epoch 2001 gives 1.4 DN, 2.7 DN, and 23 DN, respectively, for the short, medium, and long decay scales. Obviously the term with the 96 pixel decay length greatly dominates the CTE losses.

Comparison with Photometric CTE

It is of immediate interest to confirm the relevance of these hot pixel tails to photometric CTE. Specifically, do the observed tails represent a significant fraction of the photometric deficit? While these tails represent a reduction in photometric counts, it is not clear whether other loss processes (i.e. not probed by the tails) might dominate instead.

The above integral of the average hot pixel tail for 2002 contains a total of ~ 27 DN, which represents 8.7% of the average hot pixel brightness of 310 DN (i.e. Figure 2). Using the results of Dolphin (2002) for the similar case of 310 DN (2170 electrons), 1.5 DN background (similar to our 1800s dark frames), epoch 2002.5, and the CCD center ($y=400$) we would estimate 9.0% photometric CTE. Hence these observed tails, at least in this simple comparison, would appear to account for nearly all of the photometric deficit.

A more detailed comparison of photometric CTE and hot pixel CTE might take into account the brightness distribution of the PSF, shielding of downstream pixels, etc. But a crude calculation can at least give some indication whether we are seeing a significant fraction of the missing counts. For example, spreading the counts over a realistic PSF would tend to increase CTE losses (lower brightnesses have higher fractional losses), while shielding effects (traps already filled by the leading edge of the PSF) would tend to

1. Attempts to add a constant term to the triple exponential model has no significant impact on the results; the fit forces the constant term to zero and other parameters are unchanged.

reduce CTE losses. Hence, while the above calculation is crude, it does suggest the observed tails represents a significant fraction, if not nearly all, the photometric CTE.

Figure 5: Fit to average WFPC2 hot pixel tail for 1997.

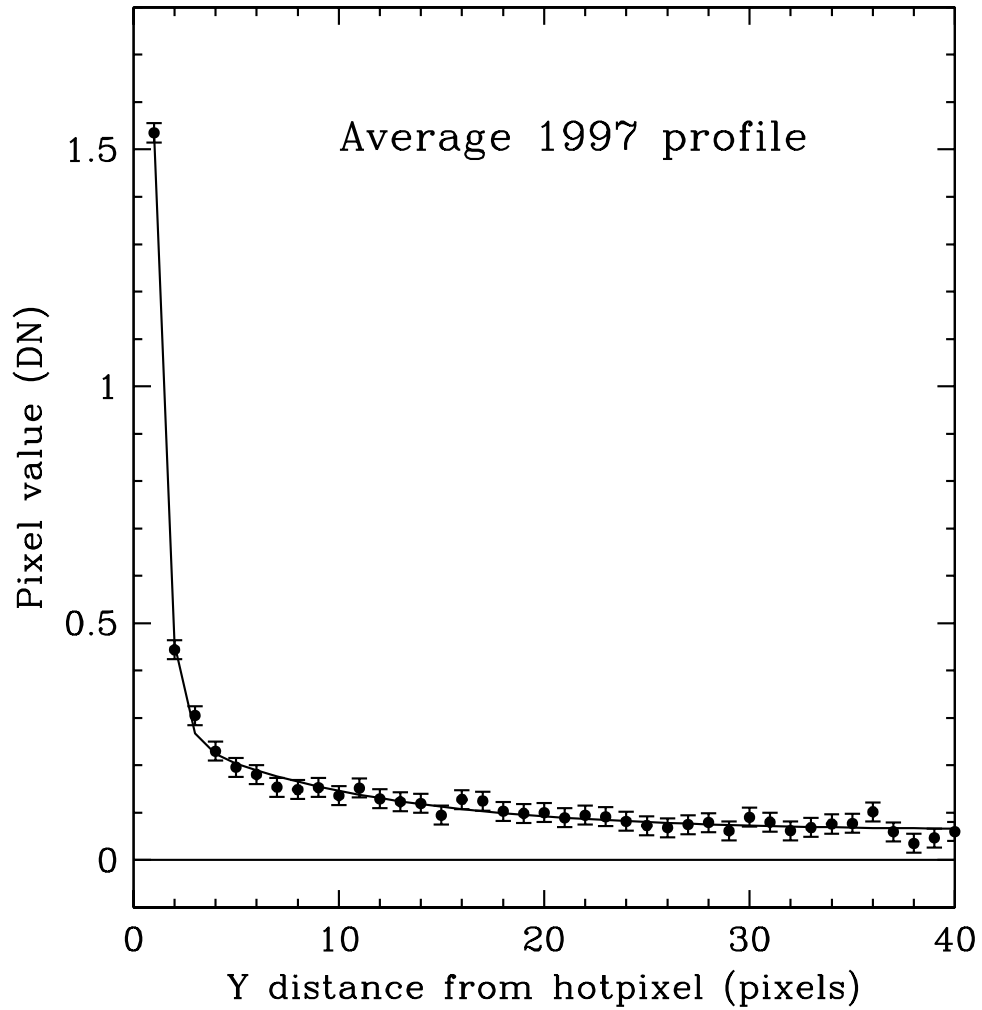


Figure 6: Fit to average WFPC2 hot pixel tail for 2001.

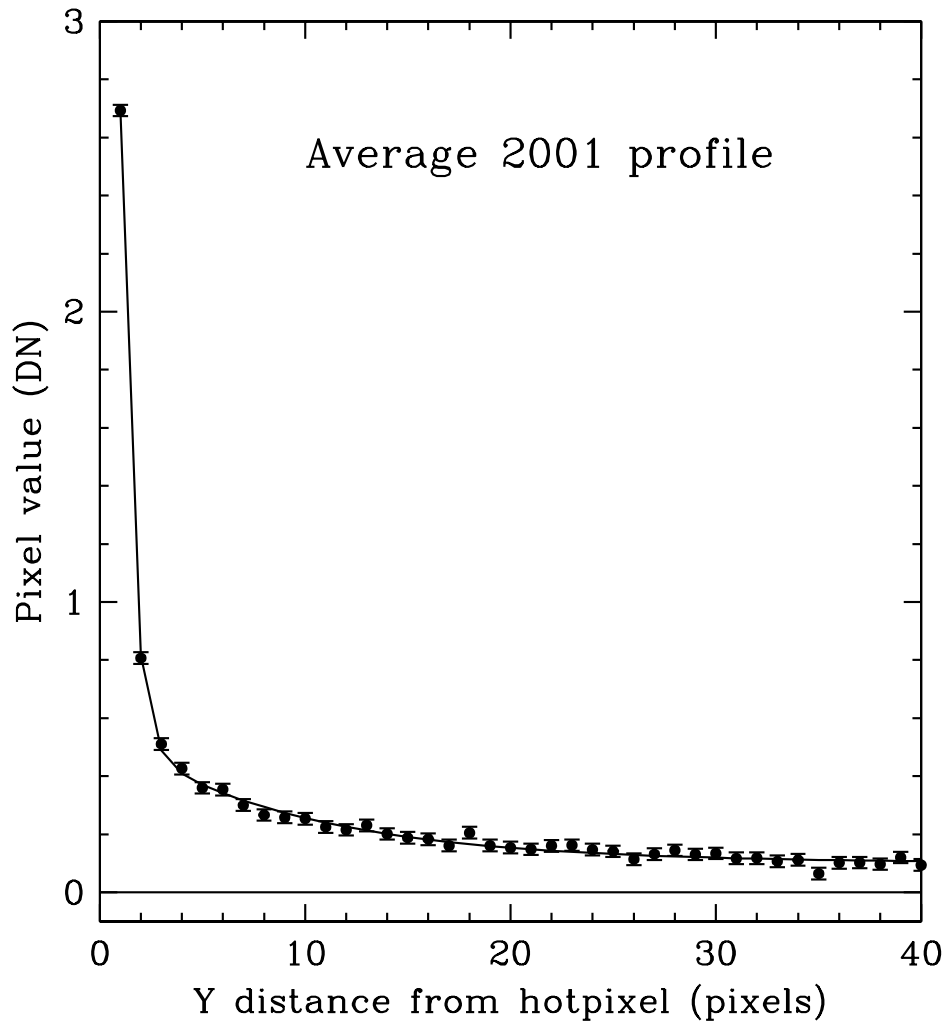
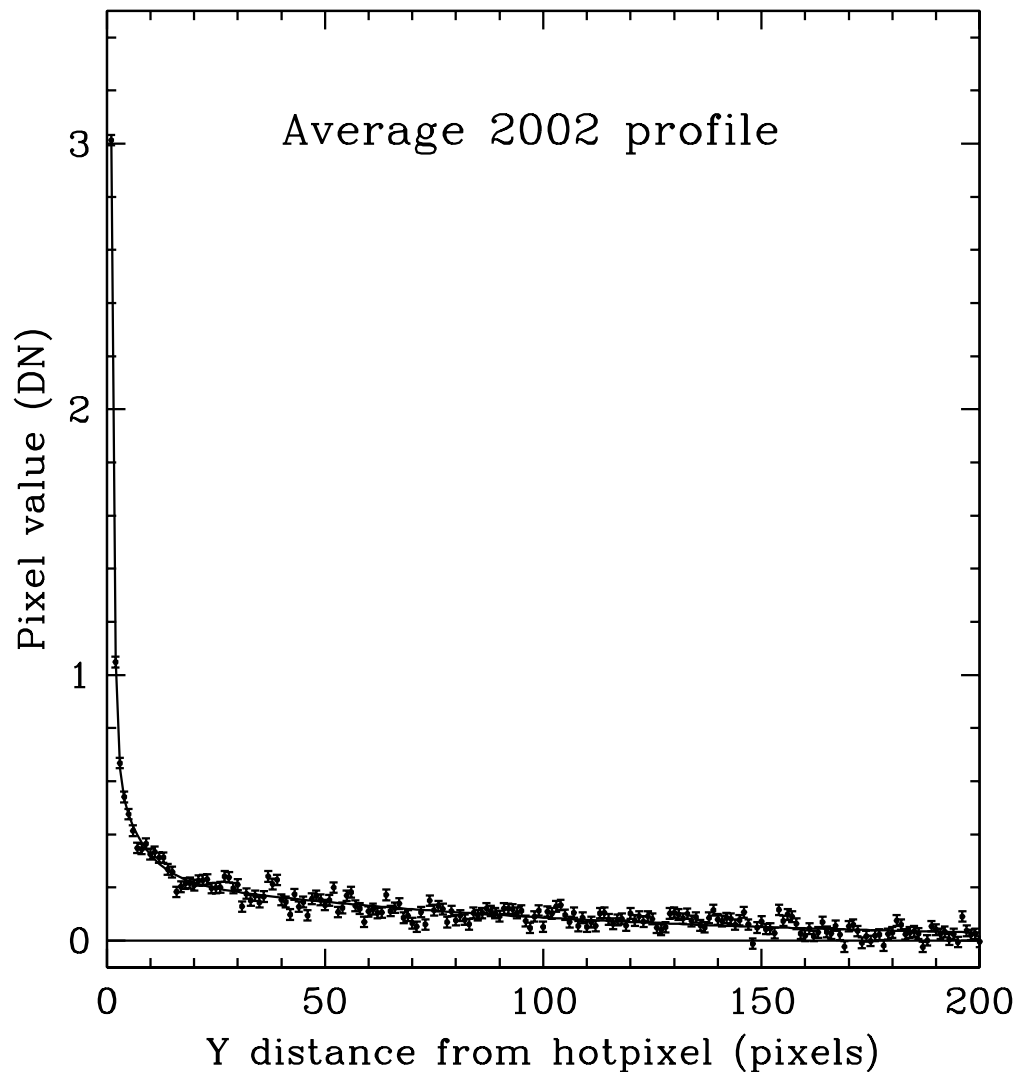


Figure 7: Fit to average WFPC2 hot pixel tail for 2002 for $\Delta y=1$ to 200 pixels.***Long-term variations***

The time dependence may be more clearly illustrated if we integrate over the pixels in the tail, and plot the integrated intensity vs. epoch. Figure 8 shows such a plot where we have summed the first 40 pixels in the tail. Each data point represents a single monthly dark. As can be seen, the strength of the tail increases approximately linearly with time. The fitted rate of increase is 0.00344 ± 0.00001 DN per day¹. Long-term variations above and

1. Of course, here we are only integrating the first 40 pixels of the tail. The increase in DN per day would be roughly a factor of two larger if we integrated the entire tail.

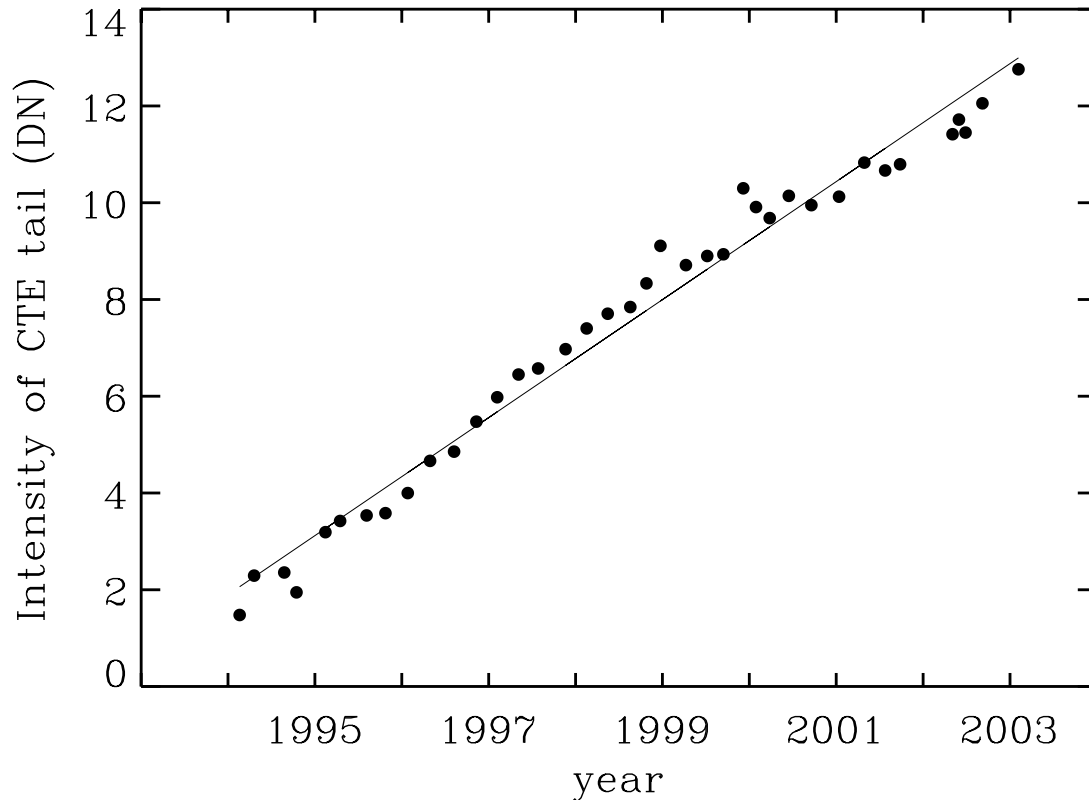
below this line may represent real changes in the rate at which the CCDs age (e.g. due to radiation damage possibly correlated with the solar cycle). We note there is a decrease in the cosmic ray flux (and presumably also in the rate of radiation damage) beginning around 1998, which is associated with the solar maximum (Mack, et al 2001).

It is interesting to compare the growth rate of the tails with that of photometric CTE. Using the epoch 1997.0 value as a reference point, the timescale for the hot pixel CTE tails to double in strength (Figure 8) is about 4.4 years. Both Whitmore, et al. (1999) and Dolphin (2002) have estimated the growth rate of CTE based on photometry of stars. Their results are embodied in the WFPC2 CTE estimator tool. Using this tool, and assuming a 310 DN star (average hot pixel brightness) and a 1.5 DN background (appropriate to the original dark frames we are using), we obtain CTE doubling times of 3.9 years and 4.4 years, respectively, for the results of Whitmore, et al. (1999) and Dolphin (2002). Hence, the growth rate of hot pixel CTE tails appears to be in remarkably good agreement with the stellar photometric CTE.

Using tails on cosmic rays, RBC99 find that the CTE tails double in intensity on a timescale of about 2.3 years (i.e. their Figure 6), which is appreciably shorter than we find¹. The difference is hard to explain. One explanation is that the different methods are sampling different brightness ranges; while the average hot pixel brightness is about 310 DN, the average cosmic ray is only ~60 DN. Hence if the growth rate depends on brightness (i.e. brightness of the cosmic ray or hot pixel), different rates might be obtained. As a check, we ran the WFPC2 CTE estimator tool #1 (Dolphin formula) for different brightnesses, and it appears the timescale increases slightly in going from 310 DN to 60 DN, not the other way around. Differences could arise since the two methods integrate over different lengths of the “tail.” Here we are integrating over 40 pixels while RBC99 uses 10 pixels. For example, there might be different components of CTE with different decay lengths and different long-term growth rates. However, our fits in the previous section show that the different exponential terms seem to grow at similar rates over time. We cannot find any simple explanation for the difference in timescales between the hot pixel and cosmic ray methods.

Since we have only integrated the tail to $y+40$ pixels, it is quite likely that we are missing some fraction of the intensity. However, to the extent that the shape of the tail remains approximately constant (as discussed above), this should not change the timescale as estimated here.

1. Their plot is for $y=800$ pixels, while ours is effectively for $y=400$ pixels, but the difference should not be important for this calculation of the timescale to double the 1997 value.

Figure 8: Integrated brightness of hot pixel CTE tail vs. epoch.

CTE vs. Y-position on CCD

The y-dependence of photometric CTE is well-known, and it is interesting to verify the same behavior for the hot pixel tails. Figure 9 illustrates the integrated brightness of the hot pixel tails vs. CCD y-coordinate for two epochs.¹ Here each data point represents the average of four monthly darks throughout the respective year, and the error bar indicates the RMS scatter of the four monthly darks. As expected, the strength of the tails increases approximately linearly with y-position on the CCD. However, an interesting new result appears -- for both epochs the y-intercept is non-zero. Apparently there is some amount of

1. For this figure we have used only hot pixels in the range $100 < \text{DN} < 400$ and integrated the first 40 pixels of the tail. It was necessary to restrict the hot pixel brightness range since the number of hot pixels in any one y-coordinate bin is relatively small, and a few very bright hot pixels in one bin would otherwise increase the scatter in the plot.

CTE even at very small $y \sim 0$ row numbers. The amount of this $y \sim 0$ CTE is quite significant - it is roughly one-fourth of that at $y=800$.¹

The photometric effects of the $y \sim 0$ CTE would depend upon its behavior with pixel brightness. If the *fraction* of counts lost were independent of brightness, then it would merely shift the photometric scale of all targets (standard stars and unknowns alike) and have no net effect. On the other hand, if it were a *fixed number* of counts, then it would behave like a photometric offset for faint targets (i.e. similar to the so-called long vs. short effect; Casertano and Mutchler 1998, Whitmore and Heyer 2002). This effect would not appear in the usual photometric CTE monitors, since those observations examine the *differences* between counts for a target moved to various locations on the CCD, and not the absolute number of counts.

It is interesting to speculate on the cause of the CTE at $y \sim 0$. For example, if it were caused by a problem with the waveforms used to clock charge into the serial register, we might expect the entire effect to be confined to the first pixel above the hot pixel. In Figure 10 we have separately plotted the 2001 results for the first pixel above the hot pixel, and for the remaining tail integrated from $\Delta y = 2$ to $\Delta y = 40$. It is clear that the CTE at $y \sim 0$ is not from the first pixel in the tail, but appears to lie farther out in the tail. This behavior is more consistent with a trapping process -- apparently a significant amount of charge is being trapped either at the location where the image is exposed, or in the region between the chip and the serial register.

The amount of charge we see in the tails at $y \sim 0$ is at least roughly consistent with the observed long vs. short effect in a simplistic model. For example, consider a model where the losses occur entirely at the pixels where the image is exposed. The mean hot pixel intensity of 310 DN is roughly what would be seen in the central pixel of an average star on the WFC with 1100 total DN (e.g. Biretta, et al. 2002, Table 5.4). If we assume each pixel in the star image loses the same 3 DN (Figure 9 interpolated to 1997), then the total loss in a 2 pixel radius aperture is about 38 DN or 0.034 magnitude. This is at least in crude agreement with the long vs. short effect observed by Casertano and Mutchler (1998); their Figure 9 gives Δm of 0.025 magnitude for ~ 1000 DN stellar images. Of course, a more complex model might take into account different DN losses in different pixels of the PSF, etc. For example, if fainter pixels in the PSF had < 3 DN loss, the predicted effect would be smaller and closer to that observed. In any case, there is at least rough agreement with the observed long vs. short effect.

1. The serial or X-CTE has no impact on this component of Y-CTE observed at $y \sim 0$. This is because we are directly measuring counts in the y -tail. We are *not* measuring some deficit or difference in counts that might be explainable as X-CTE.

Figure 9: Integrated brightness of CTE tail vs. CCD y-coordinate (row) at two epochs.

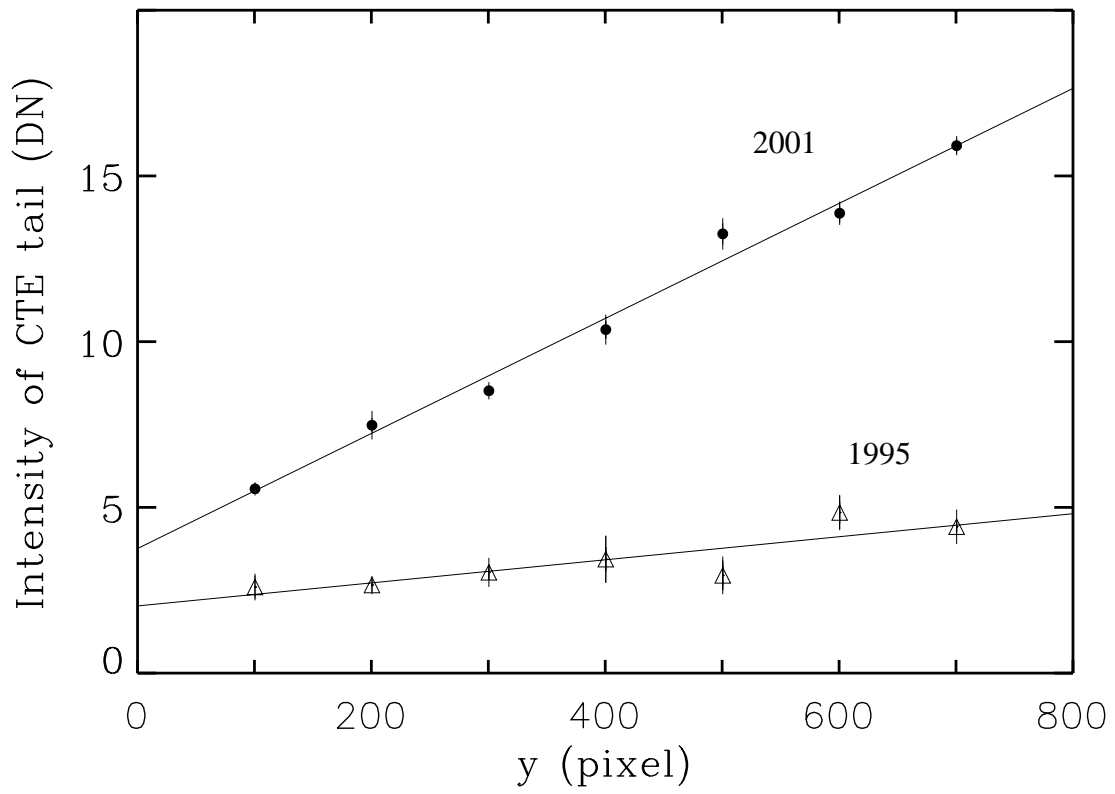
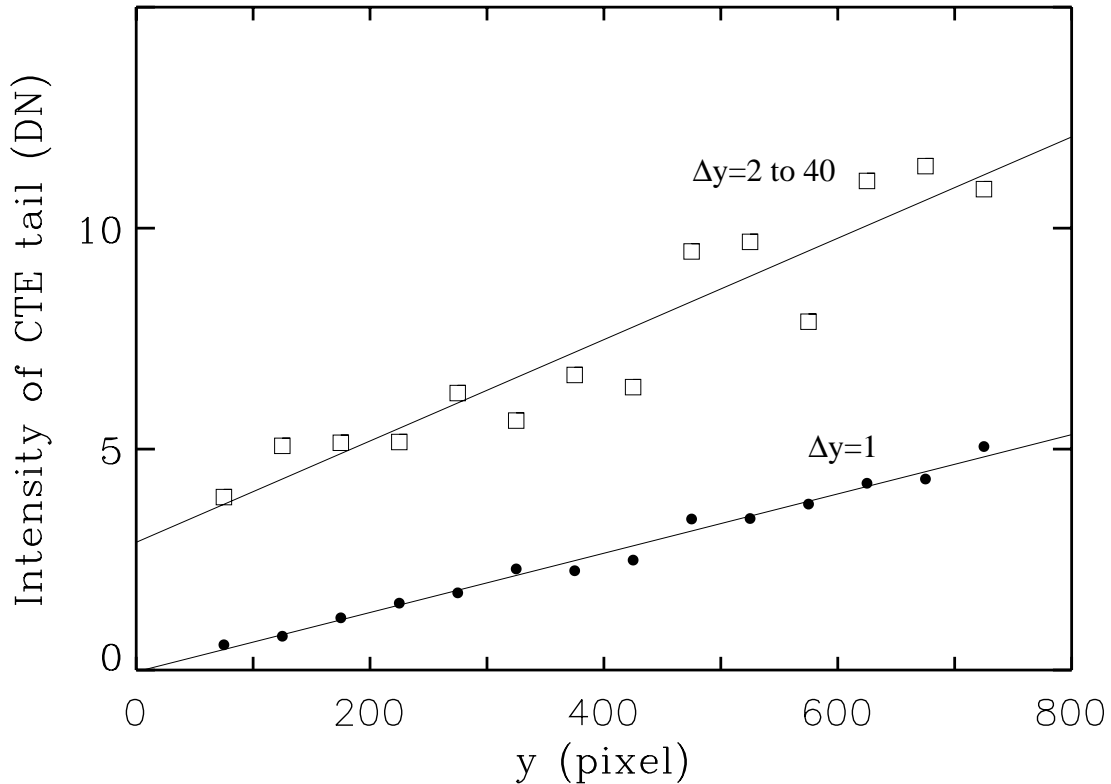


Figure 10: Brightness of CTE tail vs. CCD y-coordinate for epoch 2001. The first pixel in the tail ($\Delta y=1$) and integral of remaining tail ($\Delta y=2$ to $\Delta y=40$) are plotted separately. The plot is somewhat noisy since only one month of data is used along with narrow bins.



CTE vs. Hot Pixel Brightness

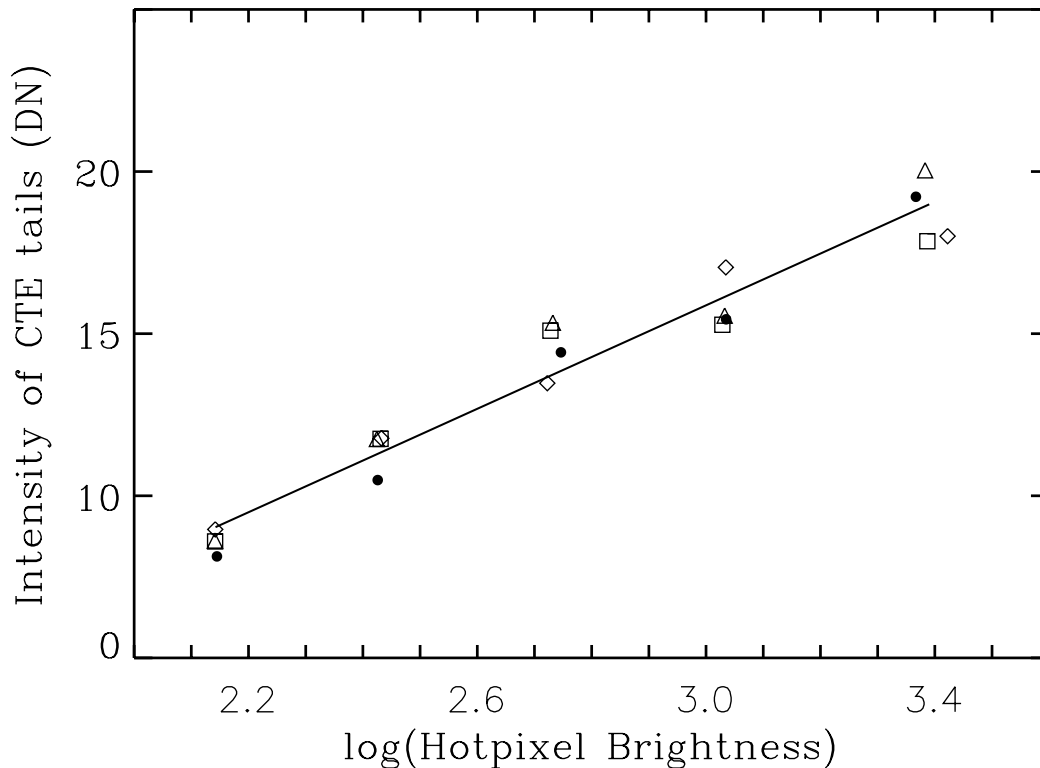
It is interesting to ask how the integrated counts in the hot pixel tail vary with hot pixel brightness. For example, this information could potentially be used to predict the CTE for a general astronomical scene by computing the tail expected for each pixel. In Figure 11 we plot hot pixel brightness against the integrated counts in the tail. We have divided up the hot pixels into five logarithmic brightness ranges, computed the average integrated counts in the tails for each range, and plotted against the average hot pixel brightness. This was done separately for four different monthly darks in 2001; a different plotting symbol is used for each of the four darks. After trying several different plots, we found that plot-

ting the tail intensity against the log of the hot pixel brightness gave the most linear relationship; the results are well fit by

$$\Sigma = (8.0 \pm 0.3)\log_{10}I - (8.1 \pm 0.5)$$

where Σ is the integrated counts in the hot pixel tail, and I is the hot pixel intensity in DN. Apparently the integrated counts in the tail increases only slowly as the hot pixel brightens. A factor of ten increase in hot pixel brightness in Figure 11 merely doubles the intensity of the tail.

Figure 11: [Integrated brightness of CTE tail vs. hot pixel brightness. The four plotting symbols indicate four different monthly darks from 2001. Hot pixel tails are integrated from $\Delta y=1$ to $\Delta y=40$.

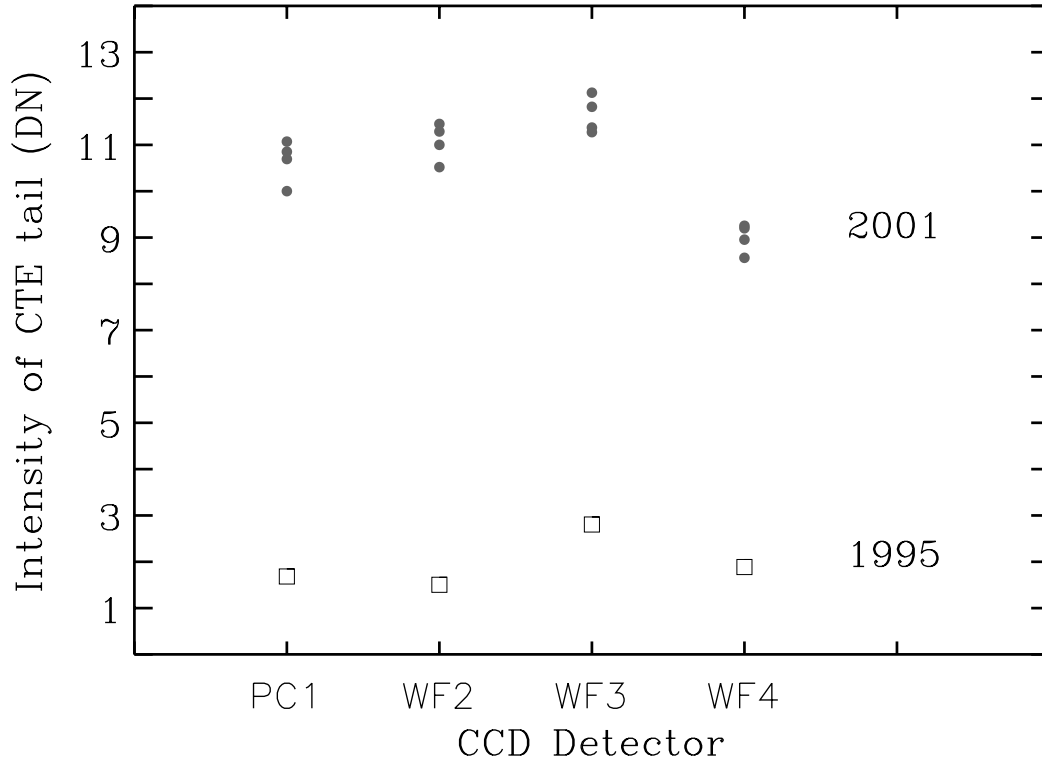


CTE vs. CCD

It seems possible that small manufacturing variances (silicon impurities, etc.) between different detectors might lead to differing susceptibilities to CTE. For example, it is conceivable that different CCDs in an instrument could respond differently to radiation damage and hence develop CTE to differing degrees. In Figure 12 we plot the integrated intensity of the hot pixel tail separately for the four WFPC2 detectors. For 2001 four different monthly darks are plotted separately in order to give an indication of the uncertainties. It seems that the WF4 detector has about 20% less CTE than the other three, and the difference appears quite significant¹. Also, WF3, which is the default detector, appears to have the highest CTE of the four. One might ask if these differences were somehow related to differences in dark current, but WF3 and WF4 have nearly identical dark currents (Mack, et al. 2001, Figure 1). If these differences between the CCDs are verified through more detailed studies, there might be some future benefit to changing default detectors for WFPC2.

1. The average hot pixel brightnesses are very similar between the CCDs, and cannot account for the differences in integrated tail intensities.

Figure 12: Integrated brightness of CTE tail vs. CCD detector. Four different monthly darks are plotted for epoch 2001. Hot pixel tails are integrated from $\Delta y=1$ to $\Delta y=40$.



Summary and Future

We have examined hot pixel tails as a potential probe of CTE effects. Specifically we find that:

1. The strength of the tails increases approximately linearly with CCD row number.
2. The strength of the hot pixel tails increases over time in a manner essentially identical to that of the photometric CTE losses; the doubling time is ~ 4.4 years.
3. The counts in the tails are quantitatively similar to the photometric CTE losses.
4. The shape of the tails appears relatively constant over time, with most of the counts falling in a component having a $1/e$ decay scale of ~ 96 pixels.
5. The strength of the tails increases slowly with hot pixel brightness -- roughly in proportion to $\log_{10}(\text{brightness})$.
6. A new result, is that there appears to be significant tails (i.e. CTE losses) even at row zero on the CCD. These losses could account for the long vs. short effect, and in fact are quantitatively similar.
7. And finally, there is evidence of chip-to-chip variations in the amount of CTE, with WF4 having the least CTE.

Results (1-3) above suggest that these hot pixel tails are caused by the same process as photometric CTE. Moreover, the quantitative similarity between the tails and missing photometric counts suggests they are probably one and the same. Hence these hot pixel tails should offer an useful laboratory for understanding CTE effects at the pixel level.

So far we have only explored hot pixels in existing dark frames -- it would be useful to examine dependencies on background light, such as found in typical science images. Such study might use science images themselves (assuming relatively empty images), or use pre-flashed dark frames. A better understanding of complex pixel-level effects (e.g. shielding) which might occur in stellar PSFs and extended targets will also be needed before one can accurately model and predict detailed CTE effects in real images. The technique outlined herein should also have obvious applicability to other space-based CCD detectors (e.g. ACS, WFC3, etc.).

Acknowledgement

We thank Ron Gilliland for a critical reading of this report.

References

Baggett, S., Biretta, J., and Hsu, J.C., 2002, "Update on Charge Trapping and CTE Residual Images in WFPC2," WFPC2 Instrument Science Report 00-03.

Biretta, J., Ritchie, C., and Rudloff, K., 1995, "A Field Guide to WFPC2 Image Anomalies," WFPC2 Instrument Science Report 95-06.

Biretta, J., and Mutchler, M., 1997, "Charge Trapping and CTE Residual Images in the WFPC2 CCDs," WFPC2 Instrument Science Report 97-05.

Biretta, J., et al., 2002, WFPC2 Instrument Handbook.

Bristow, P., Alexov, A., Kerber, F., and Rosa, M., 2002, "Modelling Charge Transfer on the STIS CCD," in *2002 HST Calibration Workshop*.

Casertano, S., and Mutchler, M., 1998, "The Long vs. Short Anomaly in WFPC2 Images," WFPC2 Instrument Science Report 98-02.

Dolphin, A., http://www.noao.edu/staff/dolphin/wfpc2_calib/

Heyer, I., 2001, "The WFPC2 Photometric CTE Monitor," WFPC2 Instrument Science Report 2001-09.

Mack, J., Biretta, J., Baggett, S., Proffitt, C., 2001, "WFPC2 Dark Current vs. Time," WFPC2 Instrument Science Report 2001-05.

Riess, A., Biretta, J., and Casertano, S., 1999, "Time Dependence of CTE from Cosmic Ray Tails," WFPC2 Instrument Science Report 99-04 (RBC99).

Riess, A., 2000, "How CTE Affects Extended Sources," WFPC2 Instrument Science Report 00-04.

Whitmore, B., Heyer, I., and Casertano, S., 1999, *PASP*, 111, 1559.

Whitmore, B., and Heyer, I., 2002, "Charge Transfer Efficiency for Very Faint Objects and a Reexamination of the Long-vs-Short Problem for the WFPC2," WFPC2 Instrument Science Report 2002-03.